Aerosol-mid-latitude cyclone indirect effects in observations and high-resolution simulations

Daniel T. McCoy[1], Paul R. Field[1,4], Anja Schmidt[1,2,3], Daniel P. Grosvenor[1], Frida A.-M. Bender[5], Ben J. Shipway[4], Adrian A. Hill[4], Jonathan M. Wilkinson[4], Gregory S. Elsaesser[6]

[1]University of Leeds, Leeds LS2 9JT, UK
[2]Department of Chemistry, University of Cambridge, Cambridge, CB2 1EW, UK
[3]Department of Geography, University of Cambridge, Downing Place, Cambridge CB2 3EN, UK
[4]Met Office, Fitzroy Rd, Exeter EX1 3PB, UK
[5]University of Stockholm, Svante Arrhenius Väg 16C, Sweden
[6]Department of Applied Physics and Mathematics, Columbia University and NASA Goddard Institute for Space Studies, New York, NY, USA

Correspondence to: Daniel T. McCoy (D.T.McCoy@leeds.ac.uk)

Abstract. Aerosol-cloud interactions are a major source of uncertainty in predicting 21st century climate change. Using high-resolution, convection-permitting global aquaplanet simulations we predict that increased cloud droplet number concentration (CDNC) in midlatitude cyclones will increase cyclone liquid water path (CLWP), and albedo. Insight into how to disentangle synoptic variability from cloud microphysical variability is gained by noting that variations in warm conveyor belt (WCB) moisture flux predict a large fraction of CLWP variability. In the framework of these predictions 13 years of observations from microwave radiometers as compiled in the Multisensor Advanced Climatology Liquid Water Path (MAC-LWP) dataset, along with observations from the Moderate Resolution Imaging Spectroradiometer (MODIS), Clouds and the Earth's Radiant Energy System (CERES), and reanalysis from The Modern-Era Retrospective analysis for Research and Applications, Version 2 (MERRA2) are analyzed. In keeping with the results from the convection-permitting aquaplanet simulations, cyclones that have a higher CDNC are observed to have a higher CLWP at a given WCB moisture flux. Based on a regression model to observed cyclone properties, roughly 60% of the variability in CLWP can be explained by CDNC and WCB moisture flux and a standard deviation change in CDNC is estimated on average to have 20-30% of the impact of a standard deviation change in WCB moisture flux on CLWP. The difference in cyclone albedo between the cyclones in the top and bottom third of observed CDNC is observed by CERES to be consistent with a 4.6-8.3 Wm^{-2} enhancement in upwelling shortwave within cyclones. The region responsible for this brightening is spatially concurrent with enhancement in CLWP

1

and cloud fraction in the region linked to the location of the cold front. This study indicates that the aerosol-cloud indirect effects have substantially altered clouds in extratropical cyclones in response to anthropogenic aerosol.

1. Introduction

5   The degree to which the aerosol indirect effects that result from anthropogenic aerosol emissions have acted to increase planetary albedo and mask greenhouse gas warming is highly uncertain (Andreae et al., 2005;Carslaw et al., 2013;Boucher et al., 2014;Forster, 2016). Establishing how much aerosol emitted during the 20th century has enhanced the liquid water amount and thus the albedo of midlatitude storm systems is a key step in constraining predictions of 21st century warming. Extratropical cyclones

10   play an important role in not only determining midlatitude albedo, but also the transport of moisture, heat, precipitation, and momentum (Hartmann, 2015;Catto et al., 2012;Hawcroft et al., 2012;Trenberth and Stepaniak, 2003;Schneider et al., 2006). Based on observational case-studies and modelling it is known that both the synoptic-scale atmospheric processes and much smaller scale cloud microphysical processes play a role in regulating the cyclone lifecycle (Naud et al., 2016;Grandey et al., 2013;Lu and Deng,

15   2016;Thompson and Eidhammer, 2014;Igel et al., 2013;Lu and Deng, 2015;Zhang et al., 2007).

In general for warm rain processes, enhanced aerosol that can act as cloud condensation nuclei (CCN) should enhance cloud droplet number concentration (CDNC, the first indirect, or Twomey effect) (McCoy et al., 2017b;Nakajima et al., 2001;Charlson et al., 1992;Twomey, 1977). This effect has the potential to suppress precipitation and lead to a greater retention of liquid water within the cloud (the

20   second indirect, lifetime, or Albrecht effect) (Albrecht, 1989;Gryspeerdt et al., 2016;Sekiguchi et al., 2003). Empirical studies have established some evidence supporting the existence of these effects in liquid clouds (Gryspeerdt et al., 2016;Quaas et al., 2008;Nakajima et al., 2001;Sekiguchi et al., 2003;McCoy et al., 2017b;McCoy et al., 2015;Meskhidze and Nenes, 2006), although it has been argued that compensating physical processes may offset these microphysical perturbations(Stevens and Feingold,

25   2009;Malavelle et al., 2017;Igel et al., 2013). Aerosol-cloud indirect effects have not been observed in extratropical cyclones. Here we use global high-resolution simulations and remote-sensing observations

to indicate that aerosol-cloud interactions produce an increase in the cloud liquid water content, cloud extent, and albedo of extratropical cyclones.

In section 2 we will discuss the observations, and idealized simulations of cloud responses to changes in CDNC used to disentangle the effects of aerosols and meteorology on cloud properties. In section 3 we present our analysis of our idealized aquaplanet simulation and we test the hypothesis arrived at in these simulations in the observational record. In section 4 we summarize our results and discuss how they relate to predicting 21st century climate change.

2. Methods

2.1 Cyclone compositing

Many previous studies have demonstrated the usefulness of averaging around cyclone centers to examine midlatitude behavior-including aerosol variability (Field et al., 2011;Field and Wood, 2007;Naud et al., 2016;Catto, 2016). A variety of different techniques for locating cyclone centers and compositing around elements of cyclones exist in the literature utilizing pressure fields (Jung et al., 2006;Löptien et al., 2008;Hoskins and Hodges, 2002;Field et al., 2008); geopotential height (Blender and Schubert, 2000); and vorticity (Sinclair, 1994;Hoskins and Hodges, 2002;Catto et al., 2010). In this study we utilize the methodology described in Field and Wood (2007). This algorithm locates cyclone centers based on sea level pressure (SLP) and then composites around each center. In this study we use the same constants relating to minima, slope and concavity of SLP contours as defined by Field and Wood (2007) to locate cyclone centers. As in Field and Wood (2007) SLP is resolved at 2.5°, and each composite is 4000 km across. When cyclone compositing is performed on observations only cyclone centers with 50% or more of the composite is located over ocean are considered. All observations that are over land are removed from the composite.

2.2 Observations

2.2.1 SLP

The Modern-Era Retrospective Analysis for Research and Applications version 2(Bosilovich et al., 2015) (MERRA2) daily-mean sea level pressure (SLP) was used to locate cyclone centers in the observational record from 2003-2015 using the algorithm described above.

5

2.2.2 MAC-LWP

The Multi-Sensor Advanced Climatology framework used for developing monthly cloud water products (Elsaesser et al., 2017) is adapted for use here to create diurnal-cycle corrected and bias-corrected daily datasets for total liquid water path (LWP, where path is the mass in an atmospheric column), 10-meter wind speed, and water vapor path (WVP).

10

One possible caveat in our analysis is that there may be cross-talk among the microwave emissions. That is to say, signal that should be attributed to wind or WVP could be attributed to LWP(Elsaesser et al., 2017). However, retrievals of WVP and wind speed have been shown to be unbiased relative to in situ observations and widespread cross-talk issues are unlikely (Mears et al., 2001;Wentz, 2015;Trenberth et al., 2005;Meissner et al., 2001;Elsaesser et al., 2017).

15

Because microwave radiometers must make assumptions regarding the partitioning of precipitating and non-precipitating liquid this represents a systematic uncertainty in the microwave LWP data set. To bypass this source of uncertainty we utilize the total LWP data product provided by MAC-LWP. The total LWP observations from this data set represent the precipitating and non-precipitating liquid water averaged over both cloudy- and clear-sky. In this study we define the sum of precipitating and non-precipitating LWP within the cyclone as cyclone-LWP (CLWP). It should be noted that the MERRA2 reanalysis total precipitable liquid water (the TQL data in MERRA2) was compared to the microwave CLWP as a rough indicator of how MERRA2's cyclone properties covaried with its predicted sulfate.

20

4

2.2.3 CDNC

Cloud droplet number concentration (CDNC) is the key state variable that moderates the relationship between aerosol and cloud properties such as LWP and cloud fraction (Wood, 2012). In this study we use two different data sets to describe CDNC: (1) the CDNC retrieved at cloud top by the Moderate Resolution Imaging Spectroradiometer (MODIS) (King et al., 2003;Nakajima et al., 2001;Grosvenor and Wood, 2014) and (2) 910 hPa sulfate mass from the MERRA2 reanalysis to assess the robustness of our analysis.

Retrievals of CDNC from the MODIS instrument were performed as described in Grosvenor and Wood (2014) and are the same data evaluated in McCoy et al. (2017a). In the present study, level-2 swath data (joint product) from MODIS collection 5.1 (King et al., 2003) is filtered by removing pixels with solar zenith angles greater than 65° to eliminate problematic retrievals at a pixel-level (Grosvenor and Wood (2014). The daily-mean CDNC at 1°x1° resolution is calculated from the filtered level 2 swath data and only low (cloud tops below 3.2 km), liquid clouds were used to calculate CDNC. Only 1°x1° regions where the cloud fraction exceeds 80% are considered valid (Bennartz et al., 2011) and the CDNC is calculated using the 3.7μm MODIS channel effective radius.

The second estimate of CDNC is provided by MERRA2 using sulfate mass. Previous studies have shown that MERRA2 sulfate mass is a good predictor of CDNC as observed by MODIS (McCoy et al., 2017a;McCoy et al., 2017b). Since MERRA2 aerosol assimilation does not ingest MODIS cloud properties the CDNC from MODIS should not influence MERRA2 sulfate(Randles et al., 2016). One caveat to using MERRA2 sulfate as a proxy for CDNC when investigating the cloud-aerosol lifetime effect is that MERRA2 does ingest microwave-observed rain rates up until 2009 and clear-sky microwave WVP into its reanalysis(McCarty et al., 2016). The possible influence of the assimilation of these cloud and meteorological properties into the MERRA2 reanalysis are evaluated in section 3. It should be noted that support for the usefulness of this data product has been provided by studying long-term trends related to volcanism and pollution controls. These have shown consistency between MODIS CDNC and sulfate mass from MERRA2 as well as observations of boundary-layer sulfur dioxide from the ozone monitoring instrument (OMI)(McCoy et al., 2017a).

These two datasets use independent approaches to estimate CDNC and will not be subject to the same errors in representing the true cloud microphysical state. Using estimate of CDNC from these two source will yield insight into the observational uncertainty surrounding CDNC.

2.2.5 Albedo

5   Finally, we examine changes in cyclone albedo due to changes in cloud properties. We utilize albedo from the CERES 3-hourly observations, where the albedo is for clear and cloudy regions. The decision to use all-sky albedo has been made to parallel previous studies(Bender et al., 2017;Bender et al., 2016;Engstrom et al., 2015b;Engstrom et al., 2015a) and has the benefit of not being sensitive to the thresholding in cloud property retrievals(Marchand et al., 2010) and potentially allowing examination of

10 broken cloud cover, which is a prominent feature in midlatitude cyclones and has the ability to substantially influence their brightness (McCoy et al., 2017c).

The 3-hourly albedo is averaged to create a daily-mean albedo. This data is provided in the CERES SYN1DEG data set edition 4(Wielicki et al., 1996). Cloud fraction (CF) from MODIS and geostationary satellites provided in the CERES SYN1DEG data set were used to examine total cloud cover and were

15 averaged in the same way as albedo to create a daily mean cloud fraction. To calculate the shortwave (SW) forcing consistent with changing albedo the average insolation in the midlatitudes was calculated. Mean solar insolation (30°-80°) was calculated using the CERES EBAF-TOA edition 4 data set(Loeb et al., 2009).

The dependence of albedo on solar zenith angle (SZA) is well-documented and needs to be either

20 removed or treated in order to contrast variations in albedo generated by clouds across latitudes and seasons (Bender et al., 2017). The dependence of albedo on cloud fraction and SZA in 3-hourly CERES data is shown in Fig. 1. Above a SZA of 45° the albedo depends strongly on SZA. While this is a real effect of low sun angles, we are more interested in understanding the albedo of cyclones without the SZA effect. To mitigate this effect we remove observations where SZA exceeds 45° from the 3-hourly

25 observations. To examine sensitivity to this cutoff we also utilize SZA cutoffs of 30° and 60°. The effect of these different cutoffs on the dependence of albedo on CF is shown in Fig. S2.

6

2.3 Simulations

2.3.1 Aquaplanet

Two sets of simulations in the MetOffice Unified Model (UM) vn10.3 based on GA6 (Walters et al., 2017) were created to test the sensitivity of the cloud-aerosol indirect effect to model resolution in an idealized aquaplanet setting. These models were a GCM-surrogate model and a convection-permitting model. The GCM-surrogate model provides a comparison to the resolution of a typical GCM and was run at 1.89°x1.25°. It incorporated a parameterized convection scheme, but no cloud-scheme was implemented meaning that only convective and large-scale clouds were simulated. The convection-permitting model was run at 0.088°x0.059° and neither convection parametrization nor cloud scheme were used. It is accepted that using this resolution (roughly 6.8km in the midlatitudes) does put the convection-permitting simulation within the convective 'Grey Zone'. The use of simulations at this resolution presents both benefits and drawbacks. Without convection being parameterized microphysics and aerosol explicitly interact allowing the cloud system to evolve in terms of changes to the rain and the anvils of the convection as well as cloud-to-cloud interactions mediated via cold pools and modifications to the thermodynamic and moisture profiles. However, while we are able to afford global aquaplanet runs at this resolution, it is not sufficiently finely resolved to completely resolve convection (as noted above) and this may lead to unknown errors in the simulations. We acknowledge these potential shortcomings, but note that our results are able to probe process related interactions in a way that parametrized convection simulations are structurally incapable of. In terms of the mean field response of explicit convection carried out at different grid resolutions intercomparison of simulations at scales ranging from 1-16km show minimal change to the mean statistics of simulated cloud fields (Field et al., 2017) giving us some confidence that our results will not just be a product of the resolution of the simulations. Overall, we find in the following sections that both GCM-surrogate and convection permitting simulations increase CLWP as aerosol increases. The response of CLWP to aerosol in the convection-permitting simulation is more pronounced than the GCM-surrogate simulation, but does not contradict it.

Both convection-permitting and GCM-surrogate simulations were run with 70 vertical levels. The Cloud-AeroSol Interacting Microphysics (CASIM) two-moment microphysics scheme (Hill et al., 2015;Shipway and Hill, 2012;Grosvenor et al., 2017) was used for all clouds in the convection-permitting

7

simulation and for large-scale cloud cover in the GCM-surrogate simulation. Most operational climate and global numerical weather prediction models do not include aerosol-aware convection(Boucher et al., 2014), as is the case in the UM operational climate model. Sea surface temperature (SST) was held fixed in the simulations and the atmosphere was allowed to spin up for a week at low resolution and then for another week at high resolution. The SST profile used in the aquaplanet was derived from a 20-year climatology run from the UM in standard climate model configuration. The January SST was averaged with a north-south reflected version of itself and then zonally averaged to provide a symmetrical SST. The aerosol profile in the control simulation was held constant at 100 cm^{-3} in the accumulation mode at the surface up until 5km and then exponentially decreased after 5km with an e-folding of 1 km. Aerosol cloud interactions were parameterized using a simple Twomey-type parameterization(Rogers and Yau, 1989) with $CDNC = 0.5Nw^{0.25}$ with N being accumulation mode aerosol number concentration and w being updraft velocity limited such that at w=16m/s CDNC=N, and w has a minimum value of 0.1m/s. Aerosol was held constant throughout the simulation. The effects of enhanced aerosol on clouds was investigated by increasing aerosol at the surface to 2000 cm^{-3} in a channel between 30°N and 60°N (with an exponential decay after 5km with an e-folding of 1 km, as in the control simulation). Ice number was controlled using a simple temperature-dependent relationship (Cooper, 1986). Simulations were then run for 15 days.

It is important to note that an increase in CDNC with increasing CCN is guaranteed by the activation parameterization used in these simulations. However, the intention of these simulations is to evaluate the response of macrophysical cloud properties to changes in CDNC and these aquaplanet simulations should be thought of in the context of a 'fixed-CDNC' set of experiments as opposed to 'fixed-CCN' experiments. In addition to the large change in CDNC between the different sensitivity experiments a small amount of variability in CDNC is introduced by vertical velocities in excess of 0.1 m/s, as noted above. In these simulations we explore the response of the clouds in the UM treated by the CASIM cloud microphysics to changes in CDNC. A different cloud microphysics scheme would potentially yield a different lifetime effect, but our results are unlikely to be qualitatively dependent on the simplistic activation scheme chosen here.

3. Results and discussion

3.1 Observed relations between meteorology, mid-latitude cyclones, and aerosol

3.1.1 Aquaplanet simulated mid-latitude cyclones and their response to changes in CCN

Compared to the meteorological drivers of cyclone formation, aerosol-cloud interactions are

5   subtle and difficult to observe. However, by using model simulations we can add or remove aerosol to disentangle aerosol-induced alterations to midlatitude storm cloud properties from the meteorology driving them. We created a suite of simulations in the MetOffice Unified Model (UM) that explores aerosol-cloud interactions as described in the methods section. Because the focus of this study is to understand maritime, midlatitude storms the model has no land surface (an aquaplanet) allowing an

10   unbroken storm track providing more cyclones to be analyzed without the complications of landmasses on their evolution. A control simulation and enhanced aerosol simulation were run at each resolution to see how cyclones differed when aerosol was increased. In the control simulation aerosol concentration was set at a value of 100 cm^{-3} near the surface and in the enhanced aerosol simulation the accumulation mode aerosol concentration was set to 2000 cm^{-3} near the surface in the 30°N-60°N latitude band. Only

15   liquid droplets are directly affected by the aerosol changes. For ice, number concentrations followed a simple temperature-dependent relationship, which is also not unusual of a GCM participating in the CMIP. Minimal impact is made on ice concentrations through variations to CCN (hence small changes to LW). We do not vary parametrizations that control the ice number when we vary CCN.

To understand the contributions of aerosol and meteorology to cyclones we need to characterize

20   what constitutes a cyclone. Cyclone centers were identified using sea level pressure (SLP) in keeping with previous studies (Field and Wood, 2007) as described in the methods section.

Considerable research has been devoted to investigating the dependence of cyclone properties on meteorology using cyclone composites(Catto, 2016). One that has been found to be particularly useful is the so-called warm conveyor belt (WCB) metric   (Field and Wood, 2007;Pfahl and Sprenger,

25   2016;Harrold, 1973). This relies on a simple model of cyclone development as described in Harrold (1973) and is calculated as the product of cyclone-mean wind speed and water vapor path multiplied by a constant describing the width of the warm conveyor belt as defined in Field and Wood (2007). It should be noted that cyclone mean here and in the rest of this article refers to an average taken within a 2000km

radius of the cyclone center. WCB moisture flux is a proxy for the moisture flux ingested by the cyclone and is a good predictor of the cyclone-mean rain rate in observations and models (Field and Wood, 2007;Field et al., 2011). The relationship between WCB flux and rain rate appears to be relatively invariant as a function of model resolution in the aquaplanet simulations analyzed in this study and aerosol concentration (Fig. S3). This is also supported by analysis of other GCMs(Field et al., 2011). Use of this metric is particularly useful in the context of our analysis because it can be measured by microwave radiometer allowing us to readily compare simulations and observations.

Essentially, once in equilibrium, the water mass flux that goes into the cyclone must be precipitated out. The perturbed aerosol environment reduces the efficiency of warm rain production for a given water path and therefore should lead to a higher equilibrium water path for a given mean rain rate or WCB flux. It is interesting to note that the frozen water path in the cyclones did not change between control and enhanced aerosol experiments, indicating that this aerosol-cyclone indirect effect acts through the warm rain process within these aquaplanet simulations (Fig. S4). Casting our analysis as a function of WCB moisture flux means that we are investigating cyclone responses to changes in CDNC at a set precipitation rate. One possibility is that this framework will prove expedient to our analysis of lifetime effects in cyclones given the divergence in precipitation responses in previous studies, ranging from intensification of precipitation (Zhang et al., 2007;Thompson and Eidhammer, 2014;Wang et al., 2014), to unchanged precipitation(Igel et al., 2013), or suppression of precipitation(Lu and Deng, 2016).

3.1.2 Observed cyclone properties

Comparison between MAC-LWP observations of cyclone-composited CLWP and aquaplanet simulations are shown in Fig. 2. To compare cyclone composites in similar meteorology conditions the cyclone composites are shown stratified by WCB moisture flux into regimes of 1-3, 3-5, and 5-7 mm/day. These regimes are selected to include weak, relatively typical and extremely large WCB moisture fluxes. Overall, the simulations carried out at convection-permitting resolution and the observations show reasonable agreement in structure and absolute value. Both the convection-permitting and GCM-surrogate simulations generally have a lower CLWP than the observations, but this is not surprising because no cloud-scheme is used in these simulations. Use of a cloud scheme would increase the CLWP and bring

10

the simulations into better absolute agreement with observations. However, the cloud scheme would require a choice of critical relative humidity(Quaas, 2012;Grosvenor et al., 2017), which would complicate our analysis of these simulations across resolutions. The GCM-surrogate simulation has a much lower CLWP than either the convection-permitting simulations or the observations. This is also likely to be at least partially due to the lack of a cloud scheme meaning that only convection or times where the entire grid box is saturated will be cloudy. Cyclone-centric composites of MERRA2 total precipitable liquid water are shown in Fig. 2f and agree qualitatively with MAC-LWP observations, although the difference between different WCB moisture flux regimes is not as strong and the cyclones are significantly more diffuse.

One consistent behavior observed across the aquaplanet simulations and observations in Fig. 2 is the enhancement in CLWP with increasing WCB moisture flux. By stratifying the cyclones simulated in the UM at GCM-surrogate and convection-permitting resolutions by the WCB moisture flux we find that WCB moisture flux plays a significant role in determining the CLWP (Fig. 3c). As one might expect, a greater flux of moisture into the cyclone results in a larger total CLWP. Such a clear WCB-CLWP relationship provides a useful metric with which to stratify midlatitude cyclones. In this framework we can now ask: for a given WCB moisture flux, do variations in the CCN available to the cyclone and hence CDNC result in a different CLWP?

We answer this question by comparing the low and high CDNC simulations and stratifying by WCB flux. This shows that for a given WCB, higher CCN translates to a higher CLWP (Fig. 3c). The difference between the control and aerosol-enhanced simulations is more pronounced in the convection-permitting model. This may be because in the GCM-surrogate simulation aerosol-cloud interactions are not represented for convection, while in the convection-permitting simulation aerosol-cloud interactions are treated in the same way for all cloud elements. As a consequence, the aerosol-cloud indirect effect as simulated by traditional GCMs that do not include aerosol-aware convection may be systematically too weak in the midlatitudes. This is because increased model CLWP results in enhanced reflection of shortwave radiation to space (Fig. S5), although thick ice clouds may mute the enhancement of reflected shortwave radiation.

11

Our hypothesis, based on these idealized simulations, is that *enhanced CCN should enhance CLWP in midlatitude storms for a given WCB moisture flux*. In this context we now examine the observational record afforded to us by the microwave radiometer data in the MAC-LWP data set. In addition to observing CLWP, the microwave radiometer is also able to measure water vapor path and wind speed, allowing for observations of WCB moisture flux and comparison to the idealized aquaplanet simulations.

Determining whether observed midlatitude cyclones have a higher or lower CCN available is more difficult than comparing high and low CCN simulations in an idealized aquaplanet. One approach would be to use the observed cloud droplet number concentration (CDNC). This provides a good proxy for CCN (Wood, 2012), but as described in the methods section it is potentially problematic because retrieval errors relating to overlying ice cloud(Sourdeval et al., 2016), cloud heterogeneity (Grosvenor and Wood, 2014;Sourdeval et al., 2016), and low sun-angle(Grosvenor and Wood, 2014) may spuriously bias the measurements making it difficult to interpret any observed covariation between cyclone properties and CDNC. To avoid these ambiguities we take a similar approach to previous studies (Boucher and Lohmann, 1995) and use both CDNC observed by MODIS and the sulfate mass concentration at the surface simulated by MERRA2 reanalysis as a proxy for CCN (McCoy et al., 2017b;McCoy et al., 2015;McCoy et al., 2017a). This use of the sulfate mass proxy is advantageous because it is not susceptible to retrieval error and because MERRA2 does not have a parameterized cloud-aerosol indirect effect, further simplifying its interpretation as a proxy of CCN.

Using the daily mean MERRA2 SO4 we calculate a CDNC proxy within cyclones following the relationship established in previous studies (McCoy et al., 2017b). An enhancement in proxy CDNC observed by MODIS and inferred from MERRA2 occurs in the southwest quadrant that is likely to be the source of moisture and aerosol for the cyclone (Fig. S6) (Cooper et al., 2004;Naud et al., 2016;Joos et al., 2016). Based on these studies the southwest quadrant of the cyclone composited CDNC will be used to stratify cyclones by CCN and will be referred to as $CDNC_{SW}$. Note that in this study all cyclone composites are oriented so that north is toward the pole and south is toward the equator so that northern and southern hemisphere cyclones are consistently oriented.

Because of the restrictions on what retrievals of CDNC are considered reliable (Grosvenor and Wood, 2014) large regions of the cyclone composite inhabited by ice cloud may be missing, in contrast no data is missing from MERRA2 sulfate because it is a reanalysis product. Examples of cyclone composited CDNC from MODIS, MERRA2 are shown in Fig. S6ab. While MERRA2 infers enhancement in CDNC in the southwest quadrant, MODIS shows a higher CDNC in the north part of the composite, which is likely due to retrieval bias at low sun angles and from heterogeneous cloud. However, the inter-cyclone variability in both cyclone-mean CDNC and $CDNC_{SW}$ observed by MODIS and inferred from MERRA2 are in agreement (Fig. S6d) and when MERRA2 is sampled where MODIS can perform a retrieval, the pattern of CDNC within the mean cyclone composite is in better agreement (Fig. S6cd).

Using WCB moisture flux as a measure of the meteorological condition and $CDNC_{SW}$ as a measure of CCN available to the cyclone we may evaluate the observational record and compare it to the aquaplanet simulations of aerosol enhancement. When we compare the observational record of cyclone-mean CLWP by stratifying it into the top and bottom third of observed $CDNC_{SW}$ inferred from MERRA2 and observed by MODIS (Fig. 4cd) a systematic separation in mean CLWP between high and low CCN cyclones becomes apparent (Fig. 3ab).

One potential caveat to this approach is that the $CDNC_{SW}$ inferred from MERRA2 sulfate has somehow been affected by the observations ingested into the MERRA2 reanalysis to create a spurious increase in sulfate in cyclones with larger CLWP, although as we have noted earlier the mechanism by which this could happen is not clear. However, if the same procedure is applied to the total precipitable liquid in MERRA2 and if $CDNC_{SW}$ inferred from MERRA2 is used to stratify the MERRA2 cyclones into high and low $CDNC_{SW}$ then low $CDNC_{SW}$ cyclones have a higher CLWP. That is to say, they have the opposite behavior of the observations from MAC-LWP (Fig. 3d). It appears that MERRA2's reanalysis is not ingesting observations of cloud properties in such a way that it spuriously drives variations in the $CDNC_{SW}$ inferred from MERRA2 sulfate mass.

It should be noted that there is some sensitivity to whether the cyclone-mean CDNC is used to stratify the cyclones or if $CDNC_{SW}$ is used (Fig. S7ab), but the CLWP for high CDNC cyclones is still higher than the CLWP for low CDNC cyclones if the cyclone-mean CDNC is used. Additional sensitivity tests of use of the southern half of the composite and the south-east quadrant of CDNC to stratify cyclones

13

are shown in Fig. S8 and Fig. S9. Only use of the south-eastern quadrant (Fig. S9) for stratification results in large portions of the high and low CDNC cyclone population being indistinguishable within the standard error. One possibility is that identification of frontal features (Naud et al., 2012) would better allow averaging around the element of the cyclone that carries CCN into the cyclone. However, based on
5   previous flow studies of aerosol within cyclones (Joos et al., 2016;Cooper et al., 2004;Naud et al., 2016) without identification of frontal features we believe that the $CDNC_{SW}$ offers a better overall representation of the importation of CCN into the cyclone and it will be used for the remainder of the analysis.

Having examined the difference in cyclone-mean properties between high and low $CDNC_{SW}$ populations we now examine differences in cyclone-centered cloud structure between these populations.
10   The difference in cloud properties between high and low $CDNC_{SW}$ cyclones share features between observations and modelling, primarily an increase in the MAC-LWP CLWP in the south-west sector of the cyclone (Fig. 5 and Fig. 6). This increase in MAC-LWP CLWP is particularly interesting as this is the region typically inhabited by open cellular convection trailing the cold front and a major source of error in simulated cyclone properties (Bodas-Salcedo et al., 2014;Naud et al., 2014;Bodas-Salcedo et al.,
15   2012;McCoy et al., 2017d).

Examination of the differences in observed cloud extent between high and low $CDNC_{SW}$ cyclones exhibit a similar pattern of differences to CLWP with enhanced cloud cover in the south west quadrant of the composites (Fig. 7). It is also interesting to note that at high WCB moisture flux cyclones with high $CDNC_{SW}$ have a lower CLWP and CF in the southeast quadrant and higher CLWP and CF in the
20   southwest quadrant. Given the relatively small number of midlatitude cyclones with WCB moisture flux greater than 5 mm/day (Fig. 4a) it is unclear if this effect is robust or a statistical artifact, but does appear regardless of which $CDNC_{SW}$ data set is used.

As shown above systematic differences in cyclone coverage and liquid content seem to exist between low and high $CDNC_{SW}$ populations, but to offer a more accurate prediction of 21st century
25   climate change the key variable to constrain is the change in reflected shortwave radiation due to aerosol indirect effects (Forster, 2016;Stevens, 2015). The difference in cyclone-composited albedo observed by CERES between cyclones whose $CDNC_{SW}$ are in the top and bottom third of the population is shown in Fig. 8. Albedo increases with increasing $CDNC_{SW}$ in the western side of the cyclone and is roughly

consistent with the regions whose CLWP and CF increased (Fig. 5 and Fig. 7). Low moisture-flux cyclones (WCB<3 mm/day) show relatively little difference in albedo if MERRA2-inferred $CDNC_{SW}$ is used to stratify the observational record. However, if MODIS observations are used to stratify the record the difference in albedo is much more pronounced across all WCB moisture flux categories. Overall, the consistency in differences in CLWP, cloud fraction, and albedo support the idea that the difference in albedo between low and high $CDNC_{SW}$ cyclones is at least partially due to changes in cloud macrophysics as opposed to purely changing cloud microphysics (CDNC) or aerosol direct effects. Differences in simulated albedo between high and low CCN simulations bear some general similarities to the observations (Fig. 9) although albedo increases are much more uniform throughout the entire cyclone region. This may reflect the extremely large difference in CCN imposed on the simulations leading to a saturation of the aerosol-cloud lifetime effect.

   Having inspected the differences in the structure of cloud properties and albedo between high and low CDNCSW populations we will now examine the difference in cyclone-mean albedo. To do this we first divide the high and low CDNCSW populations into 15 equal quantiles of WCB moisture flux. The mean albedo and the standard error in the mean ($SE = \sigma n$) (where sigma is standard deviation and n is the total number of observations) are calculated in each quantile (Fig. 10a). The mean albedo is higher for the high $CDNC_{SW}$ population. When MODIS is used to retrieve CDNC the albedo is on average 0.03 higher in the high $CDNC_{SW}$ population. If MERRA2 inferred CDNC is used then the cyclone albedo is only higher for the high $CDNC_{SW}$ population when WCB moisture fluxes is greater than 2 mm/day.

   To calculate the difference in mean albedo between high and low $CDNC_{SW}$ populations in each quantile the quantile-average WCB moisture flux needs to be examined. Because the mean WCB in each quantile may be slightly different for the high and low $CDNC_{SW}$ populations the mean and standard error for the high $CDNC_{SW}$ population is linearly interpolated so that the mean WCB moisture flux in each quantile between the low and high $CDNC_{SW}$ populations. For each quantile the standard error in the difference is propagated as $SE_{High-Low} = \sqrt{SE_{High}^2 + SE_{Low}^2}$. The average difference in albedo across quantiles is taken. The associated standard error in the averaged difference in albedo is calculated as

$\sqrt{\sum \frac{SE_i^2}{15^2}}$. The difference and standard error in the difference between high and low $CDNC_{SW}$ populations as a function of WCB is shown in Fig. 10b.

To calculate the difference in terms of a radiative flux the difference in albedo is multiplied by the annual mean climatological downwelling SW associated with the CERES EBAF-TOA data set between 30°-80°. This yields a difference in reflected SW between high and low $CDNC_{SW}$ populations of 8.30±0.31 Wm^{-2} if MODIS is used to stratify cyclones and 4.62±0.33 Wm^{-2} if MERRA2-inferred CDNC is used (Fig. 10b). This result does show some sensitivity to the maximum solar zenith angle considered acceptable for the 3-hourly CERES data. A maximum SZA of 30° yields values of 5.58±0.48 and 4.23±0.63 Wm^{-2} for MODIS and MERRA2-inferred CDNC, respectively (Fig. S10)). A maximum SZA of 60° yields values of 6.50±0.27 Wm-2 and 2.88±0.28 Wm^{-2} (Fig. S11). If all SZAs are included this reverses the position of the low and high $CDNC_{SW}$ cyclones (Fig. S12). However, the inclusion of all SZAs observed by CERES includes albedos where the SZA effect dominates so low CF and low CLWP cyclones can be considerably higher albedo (Fig. S1). Again, this effect is physical, but including the seasonal cycle and position of cyclones in our analysis via this effect makes it difficult to disentangle the very pronounced SZA effect from changes associated with changes in cloud properties. It is also worth noting that the difference in albedo estimated using MERRA2 SO4 to stratify cyclones is likely to have a larger sensitivity to the maximum SZA cutoff used because MODIS CDNC retrievals are not possible when the SZA exceeds 65° and so cyclones in winter are not considered in the analysis, while MERRA2 SO4 allows these cyclones to be examined.

3.1.3 Regression model of CLWP

Given the pervasiveness of the relationships between CLWP, $CDNC_{SW}$, and WCB we create a simple regression model of CLWP to allow us to assess how much of the variance is explained by these parameters and the relative importance of 'meteorology' and 'aerosol'. The relationship between CLWP, WCB and $CDNC_{SW}$ shows differing behavior as a function of $CDNC_{SW}$ with a stronger increase in CLWP for a given increase in $CDNC_{SW}$ in more pristine (low $CDNC_{SW}$) storms (Fig. 11, Fig. S13). Using the observational record from 2003-2015 we train a regression model

16

$$CLWP = aWCB^b CDNC_{SW}^c - d \qquad (1)$$

where WCB is in units of mm/day, CDNC is in cm^{-3}, and CLWP is in mm. Coefficients for the regression model trained using $CDNC_{SW}$ observed by MODIS and inferred from MERRA2 sulfate are shown in Table 1. The regression model explains 62%-67% of the variance in the observed CLWP.

5   It is interesting to consider how susceptible CLWP is to a perturbation in $CDNC_{SW}$ in the space of WCB and $CDNC_{SW}$. That is to say, what parts of the cyclone population would be more susceptible to changes in CDNC and which are effectively only sensitive to meteorology in the context of equation 1? We illustrate this by examining the response of equation 1 to typical perturbations in each predictor. In the context of this illustrative analysis a standard deviation is considered a typical perturbation. The

10 standard deviation in WCB and $CDNC_{SW}$ are calculated across the data record. The coefficients for equation 1 shown in Table 1 are then used to calculate the change in CLWP for a standard deviation increase in WCB and $CDNC_{SW}$. This illustrates the relative importance of changes in aerosol (as exemplified by $CDNC_{SW}$) and changes in meteorological environment (as exemplified by WCB moisture flux) and is visualized in Fig. 12 for equation 1 trained using MODIS $CDNC_{SW}$.

15   Based on the simple visualization in Fig. 12 (and Fig. S14 if the $CDNC_{SW}$ inferred from MERRA2 is used to train the model) we can see that changes in CLWP for very pristine ($CDNC_{SW}<60cm^{-3}$), large moisture flux cyclones (WCB>4 mm/day) due to unit standard deviation perturbation in $CDNC_{SW}$ are estimated to be as large as 50% of those from a standard deviation perturbation in meteorology (WCB flux), while very polluted ($CDNC_{SW}>120cm^{-3}$), small moisture flux cyclones (WCB<2mm/day) are

20 nearly insensitive to changes in $CDNC_{SW}$. This result is in keeping with Carslaw et al. (2013), which demonstrated the importance of understanding low CCN regions to constrain the aerosol-cloud indirect effect. The sensitivity of our regression model to CDNC changes supports the importance of understanding CCN sources in remote, pristine regions. Averaged over the observational record, the mean relative contribution of aerosol changes to the variability in CLWP is 20% (30% if MERRA2-

25 inferred $CDNC_{SW}$ is used) based on the observed distribution of cyclones in $CDNC_{SW}$ and WCB space.

4. Conclusions

Insight gained by the investigation of high-resolution, convection-permitting idealized global simulations has allowed us to hypothesize that cyclone liquid water path is substantially influenced by aerosol perturbations providing an important key to evaluating and constraining the second indirect effect in models and offering a more tightly-constrained estimate of anthropogenic radiative forcing and of 21st century warming.

Based on the idealized simulations and analysis of observations shown here we have developed and tested the hypothesis that *enhanced CCN should enhance CLWP in midlatitude storms for a given WCB moisture flux*. It is possible that this effect is not constrained to midlatitude cyclones and we may speculate that clouds in other regimes whose rain rate is the same have a higher LWP with increasing aerosol.

A regression model representation of CLWP as a function of WCB moisture flux and CDNC in the southwest quadrant of the cyclone ($CDNC_{SW}$) explains approximately 60% of observed variability in CLWP. Based on this regression model we infer that, as one would expect, meteorology (as characterized by WCB moisture flux) dominates CLWP variability. However, the response of CLWP as inferred by the regression model to a standard deviation change in $CDNC_{SW}$ can be a significant fraction of the response to a standard deviation in WCB moisture flux (Fig. 12). A mean relative contribution of $CDNC_{SW}$ variability to CLWP variability of 20-30% is estimated.

Comparison of cyclone properties in the top and bottom third of the $CDNC_{SW}$ population correspond to different mean CLWP for a given WCB moisture flux, but also significant changes in cyclone cloud fraction and albedo. Differences in the cyclone-mean albedo observed by CERES equate to an in-cyclone enhancement in outgoing top of atmosphere shortwave between 4.6 Wm^{-2} and 8.3 Wm^{-2} if the change in albedo is scaled by the annual-mean downwelling shortwave between $30°$-$80°$ (Fig. 10).

An aerosol indirect effect on the clouds in midlatitude storms has been predicted by simulations of the North Pacific (Wang et al., 2014;Joos et al., 2016), and observed in the intensification of the North Pacific storm track(Zhang et al., 2007), but this is the first time it has been demonstrated using observations from across the extratropics.

18

10 **References**

Albrecht, B. A.: Aerosols, Cloud Microphysics, and Fractional Cloudiness, Science, 245, 1227-1230, 10.1126/science.245.4923.1227, 1989.

Andreae, M. O., Jones, C. D., and Cox, P. M.: Strong present-day aerosol cooling implies a hot future, Nature, 435, 1187, 2005.

Bender, F. A. M., Engström, A., and Karlsson, J.: Factors Controlling Cloud Albedo in Marine Subtropical Stratocumulus Regions in
15 Climate Models and Satellite Observations, Journal of Climate, 29, 3559-3587, 10.1175/jcli-d-15-0095.1, 2016.

Bender, F. A. M., Engström, A., Wood, R., and Charlson, R. J.: Evaluation of Hemispheric Asymmetries in Marine Cloud Radiative Properties, Journal of Climate, 30, 4131-4147, 10.1175/JCLI-D-16-0263.1, 2017.

Bennartz, R., Fan, J., Rausch, J., Leung, L. R., and Heidinger, A. K.: Pollution from China increases cloud droplet number, suppresses rain over the East China Sea, Geophys. Res. Lett., 38, n/a-n/a, 10.1029/2011GL047235, 2011.

20 Blender, R., and Schubert, M.: Cyclone tracking in different spatial and temporal resolutions, Monthly Weather Review, 128, 377-384, 2000.

Bodas-Salcedo, A., Williams, K. D., Field, P. R., and Lock, A. P.: The Surface Downwelling Solar Radiation Surplus over the Southern Ocean in the Met Office Model: The Role of Midlatitude Cyclone Clouds, Journal of Climate, 25, 7467-7486, 10.1175/jcli-d-11-00702.1, 2012.

25 Bodas-Salcedo, A., Williams, K. D., Ringer, M. A., Beau, I., Cole, J. N. S., Dufresne, J. L., Koshiro, T., Stevens, B., Wang, Z., and Yokohata, T.: Origins of the Solar Radiation Biases over the Southern Ocean in CFMIP2 Models, Journal of Climate, 27, 41-56, 10.1175/jcli-d-13-00169.1, 2014.

Bosilovich, M., Akella, S., Coy, L., Cullather, R., Draper, C., and Gelaro, R.: MERRA-2. Initial evaluation of the climate, Tech. Rep. Ser., Global Modeling and Data Assimilation, RD Koster, ed., NASA/TM-2015-104606, 2015.

30 Boucher, O., and Lohmann, U.: The sulfate-CCN-cloud albedo effect, Tellus B, 47, 281-300, 10.1034/j.1600-0889.47.issue3.1.x, 1995.

Boucher, O., Randall, D. A., Artaxo, P., Bretherton, C., Feingold, G., Forster, P. M., Kerminen, V.-M., Kondo, Y., Liao, H., Lohmann, U., Rasch, P., Satheesh, S. K., Sherwood, S. C., Stevens, B., and Zhang, X. Y.: Clouds and Aerosols
Climate Change 2013 - The Physical Science Basis, Cambridge University Press, 2014.

Carslaw, K. S., Lee, L. A., Reddington, C. L., Pringle, K. J., Rap, A., Forster, P. M., Mann, G. W., Spracklen, D. V., Woodhouse, M. T.,
35 Regayre, L. A., and Pierce, J. R.: Large contribution of natural aerosols to uncertainty in indirect forcing, Nature, 503, 67-71, 10.1038/nature12674, 2013.

Catto, J. L., Shaffrey, L. C., and Hodges, K. I.: Can climate models capture the structure of extratropical cyclones?, Journal of Climate, 23, 1621-1635, 2010.

Catto, J. L., Jakob, C., Berry, G., and Nicholls, N.: Relating global precipitation to atmospheric fronts, Geophysical Research Letters, 39,
40 n/a-n/a, 10.1029/2012GL051736, 2012.

Catto, J. L.: Extratropical cyclone classification and its use in climate studies, Reviews of Geophysics, 54, 486-520, 10.1002/2016RG000519, 2016.

19

Charlson, R. J., Schwartz, S. E., Hales, J. M., Cess, R. D., Coakley, J. A., Hansen, J. E., and Hofmann, D. J.: Climate Forcing by Anthropogenic Aerosols, Science, 255, 423-430, 10.1126/science.255.5043.423, 1992.

Cooper, O. R., Forster, C., Parrish, D., Trainer, M., Dunlea, E., Ryerson, T., Hübler, G., Fehsenfeld, F., Nicks, D., Holloway, J., de Gouw, J., Warneke, C., Roberts, J. M., Flocke, F., and Moody, J.: A case study of transpacific warm conveyor belt transport: Influence of merging airstreams on trace gas import to North America, Journal of Geophysical Research: Atmospheres, 109, n/a-n/a, 10.1029/2003JD003624, 2004.

Cooper, W. A.: Ice initiation in natural clouds, in: Precipitation Enhancement—A Scientific Challenge, Springer, 29-32, 1986.

Elsaesser, G. S., O'Dell, C. W., Lebsock, M. D., Bennartz, R., Greenwald, T. J., and Wentz, F. J.: The Multi-Sensor Advanced Climatology of Liquid Water Path (MAC-LWP), Journal of Climate, 0, null, 10.1175/jcli-d-16-0902.1, 2017.

Engstrom, A., Bender, F. A. M., Charlson, R. J., and Wood, R.: The nonlinear relationship between albedo and cloud fraction on near-global, monthly mean scale in observations and in the CMIP5 model ensemble, Geophys. Res. Lett., 42, 9571-9578, 10.1002/2015gl066275, 2015a.

Engstrom, A., Bender, F. A. M., Charlson, R. J., and Wood, R.: Geographically coherent patterns of albedo enhancement and suppression associated with aerosol sources and sinks, Tellus, 2015b.

Field, P. R., and Wood, R.: Precipitation and cloud structure in midlatitude cyclones, Journal of Climate, 20, 233-254, 10.1175/jcli3998.1, 2007.

Field, P. R., Gettelman, A., Neale, R. B., Wood, R., Rasch, P. J., and Morrison, H.: Midlatitude Cyclone Compositing to Constrain Climate Model Behavior Using Satellite Observations, Journal of Climate, 21, 5887-5903, doi:10.1175/2008JCLI2235.1, 2008.

Field, P. R., Bodas-Salcedo, A., and Brooks, M. E.: Using model analysis and satellite data to assess cloud and precipitation in midlatitude cyclones, Quarterly Journal of the Royal Meteorological Society, 137, 1501-1515, 10.1002/qj.858, 2011.

Field, P. R., Brožková, R., Chen, M., Dudhia, J., Lac, C., Hara, T., Honnert, R., Olson, J., Siebesma, P., de Roode, S., Tomassini, L., Hill, A., and McTaggart-Cowan, R.: Exploring the convective grey zone with regional simulations of a cold air outbreak, Quarterly Journal of the Royal Meteorological Society, 143, 2537-2555, 10.1002/qj.3105, 2017.

Forster, P. M.: Inference of climate sensitivity from analysis of Earth's energy budget, Annual Review of Earth and Planetary Sciences, 44, 85-106, 2016.

Grandey, B. S., Stier, P., Grainger, R. G., and Wagner, T. M.: The contribution of the strength and structure of extratropical cyclones to observed cloud–aerosol relationships, Atmos. Chem. Phys., 13, 10689-10701, 10.5194/acp-13-10689-2013, 2013.

Grosvenor, D. P., and Wood, R.: The effect of solar zenith angle on MODIS cloud optical and microphysical retrievals within marine liquid water clouds, Atmos. Chem. Phys., 14, 7291-7321, 10.5194/acp-14-7291-2014, 2014.

Grosvenor, D. P., Field, P. R., Hill, A. A., and Shipway, B. J.: The relative importance of macrophysical and cloud albedo changes for aerosol-induced radiative effects in closed-cell stratocumulus: insight from the modelling of a case study, Atmos. Chem. Phys., 17, 5155-5183, 10.5194/acp-17-5155-2017, 2017.

Gryspeerdt, E., Quaas, J., and Bellouin, N.: Constraining the aerosol influence on cloud fraction, Journal of Geophysical Research: Atmospheres, n/a-n/a, 10.1002/2015JD023744, 2016.

Harrold, T. W.: Mechanisms influencing the distribution of precipitation within baroclinic disturbances, Quarterly Journal of the Royal Meteorological Society, 99, 232-251, 10.1002/qj.49709942003, 1973.

Hartmann, D. L.: Global physical climatology, Newnes, 2015.

Hawcroft, M. K., Shaffrey, L. C., Hodges, K. I., and Dacre, H. F.: How much Northern Hemisphere precipitation is associated with extratropical cyclones?, Geophysical Research Letters, 39, n/a-n/a, 10.1029/2012GL053866, 2012.

Hill, A. A., Shipway, B. J., and Boutle, I. A.: How sensitive are aerosol-precipitation interactions to the warm rain representation?, Journal of Advances in Modeling Earth Systems, 7, 987-1004, 10.1002/2014MS000422, 2015.

Hoskins, B. J., and Hodges, K. I.: New perspectives on the Northern Hemisphere winter storm tracks, Journal of the Atmospheric Sciences, 59, 1041-1061, 2002.

Igel, A. L., van den Heever, S. C., Naud, C. M., Saleeby, S. M., and Posselt, D. J.: Sensitivity of Warm-Frontal Processes to Cloud-Nucleating Aerosol Concentrations, Journal of the Atmospheric Sciences, 70, 1768-1783, 10.1175/JAS-D-12-0170.1, 2013.

Joos, H., Madonna, E., Witlox, K., Ferrachat, S., Wernli, H., and Lohmann, U.: Effect of anthropogenic aerosol emissions on precipitation in warm conveyor belts in the western North Pacific in winter – a model study with ECHAM6-HAM, Atmos. Chem. Phys. Discuss., 2016, 1-20, 10.5194/acp-2016-722, 2016.

Jung, T., Gulev, S. K., Rudeva, I., and Soloviov, V.: Sensitivity of extratropical cyclone characteristics to horizontal resolution in the ECMWF model, Quarterly Journal of the Royal Meteorological Society, 132, 1839-1857, 10.1256/qj.05.212, 2006.

King, M. D., Menzel, W. P., Kaufman, Y. J., Tanre, D., Bo-Cai, G., Platnick, S., Ackerman, S. A., Remer, L. A., Pincus, R., and Hubanks, P. A.: Cloud and aerosol properties, precipitable water, and profiles of temperature and water vapor from MODIS, Geoscience and Remote Sensing, IEEE Transactions on, 41, 442-458, 10.1109/TGRS.2002.808226, 2003.

Loeb, N. G., Wielicki, B. A., Doelling, D. R., Smith, G. L., Keyes, D. F., Kato, S., Manalo-Smith, N., and Wong, T.: Toward Optimal Closure of the Earth's Top-of-Atmosphere Radiation Budget, Journal of Climate, 22, 748-766, 10.1175/2008jcli2637.1, 2009.

20

Löptien, U., Zolina, O., Gulev, S., Latif, M., and Soloviov, V.: Cyclone life cycle characteristics over the Northern Hemisphere in coupled GCMs, Climate dynamics, 31, 507-532, 2008.

Lu, Y., and Deng, Y.: Initial Transient Response of an Intensifying Baroclinic Wave to Increases in Cloud Droplet Number Concentration, Journal of Climate, 28, 9669-9677, 10.1175/jcli-d-15-0251.1, 2015.

5   Lu, Y., and Deng, Y.: Impact of Environmental Aerosols on a Developing Extratropical Cyclone in the Superparameterized Community Atmosphere Model, Journal of Climate, 29, 5533-5546, 10.1175/JCLI-D-16-0157.1, 2016.

Malavelle, F. F., Haywood, J. M., Jones, A., Gettelman, A., Clarisse, L., Bauduin, S., Allan, R. P., Karset, I. H. H., Kristjánsson, J. E., Oreopoulos, L., Cho, N., Lee, D., Bellouin, N., Boucher, O., Grosvenor, D. P., Carslaw, K. S., Dhomse, S., Mann, G. W., Schmidt, A., Coe, H., Hartley, M. E., Dalvi, M., Hill, A. A., Johnson, B. T., Johnson, C. E., Knight, J. R., O'Connor, F. M., Partridge, D. G., Stier, P.,

10   Myhre, G., Platnick, S., Stephens, G. L., Takahashi, H., and Thordarson, T.: Strong constraints on aerosol–cloud interactions from volcanic eruptions, Nature, 546, 485-491, 10.1038/nature22974
[http://www.nature.com/nature/journal/v546/n7659/abs/nature22974.html - supplementary-information](http://www.nature.com/nature/journal/v546/n7659/abs/nature22974.html), 2017.

Marchand, R., Ackerman, T., Smyth, M., and Rossow, W. B.: A review of cloud top height and optical depth histograms from MISR,
15   ISCCP, and MODIS, Journal of Geophysical Research-Atmospheres, 115, D16206
10.1029/2009jd013422, 2010.

McCarty, W., Coy, L., R, G., A, H., Merkova, D., EB, S., M, S., and K, W.: MERRA-2 Input Observations: Summary and Assessment, Technical Report Series on Global Modeling and Data Assimilation, 46, 2016.

McCoy, D. T., Burrows, S. M., Wood, R., Grosvenor, D. P., Elliott, S. M., Ma, P.-L., Rasch, P. J., and Hartmann, D. L.: Natural aerosols
20   explain seasonal and spatial patterns of Southern Ocean cloud albedo, Science Advances, 1, 2015.

McCoy, D. T., Bender, F. A. M., Grosvenor, D. P., Mohrmann, J. K., Hartmann, D. L., Wood, R., and Field, P. R.: Predicting decadal trends in cloud droplet number concentration using reanalysis and satellite data, Atmos. Chem. Phys. Discuss., 2017, 1-21, 10.5194/acp-2017-811, 2017a.

McCoy, D. T., Bender, F. A. M., Mohrmann, J. K., Hartmann, D. L., Wood, R., and Grosvenor, D. P.: The global aerosol-cloud first
25   indirect effect estimated using MODIS, MERRA and AeroCom, Journal of Geophysical Research: Atmospheres, n/a-n/a, 10.1002/2016JD026141, 2017b.

McCoy, I. L., Wood, R., and Fletcher, J. K.: Identifying Meteorological Controls on Open and Closed Mesoscale Cellular Convection Associated with Marine Cold Air Outbreaks, Journal of Geophysical Research: Atmospheres, n/a-n/a, 10.1002/2017JD027031, 2017c.

McCoy, I. L., Wood, R., and Fletcher, J. K.: Identifying Meteorological Controls on Open and Closed Mesoscale Cellular Convection
30   Associated with Marine Cold Air Outbreaks, Journal of Geophysical Research: Atmospheres 2017d.

Mears, C., Smith, D. K., and Wentz, F. J.: Comparison of special sensor microwave imager and buoy-measured wind speeds from 1987 to 1997, Journal of Geophysical Research: Oceans, 106, 11719-11729, 2001.

Meissner, T., Smith, D., and Wentz, F.: A 10 year intercomparison between collocated Special Sensor Microwave Imager oceanic surface wind speed retrievals and global analyses, Journal of Geophysical Research: Oceans, 106, 11731-11742, 2001.

35   Meskhidze, N., and Nenes, A.: Phytoplankton and Cloudiness in the Southern Ocean, Science, 314, 1419-1423, 10.1126/science.1131779, 2006.

Nakajima, T., Higurashi, A., Kawamoto, K., and Penner, J. E.: A possible correlation between satellite-derived cloud and aerosol microphysical parameters, Geophys. Res. Lett., 28, 1171-1174, 10.1029/2000GL012186, 2001.

Naud, C. M., Posselt, D. J., and van den Heever, S. C.: Observational Analysis of Cloud and Precipitation in Midlatitude Cyclones:
40   Northern versus Southern Hemisphere Warm Fronts, Journal of Climate, 25, 5135-5151, 10.1175/jcli-d-11-00569.1, 2012.

Naud, C. M., Booth, J. F., and Del Genio, A. D.: Evaluation of ERA-Interim and MERRA Cloudiness in the Southern Ocean, Journal of Climate, 27, 2109-2124, 10.1175/jcli-d-13-00432.1, 2014.

Naud, C. M., Posselt, D. J., and van den Heever, S. C.: Aerosol optical depth distribution in extratropical cyclones over the Northern Hemisphere oceans, Geophysical Research Letters, 43, 10,504-510,511, 10.1002/2016GL070953, 2016.

45   Pfahl, S., and Sprenger, M.: On the relationship between extratropical cyclone precipitation and intensity, Geophysical Research Letters, 43, 1752-1758, 10.1002/2016GL068018, 2016.

Quaas, J., Boucher, O., Bellouin, N., and Kinne, S.: Satellite-based estimate of the direct and indirect aerosol climate forcing, Journal of Geophysical Research: Atmospheres, 113, n/a-n/a, 10.1029/2007JD008962, 2008.

Quaas, J.: Evaluating the "critical relative humidity" as a measure of subgrid-scale variability of humidity in general circulation model
50   cloud cover parameterizations using satellite data, Journal of Geophysical Research: Atmospheres, 117, n/a-n/a, 10.1029/2012JD017495, 2012.

Randles, C., AM, d. S., V, B., A, D., PR, C., V, A., H, B., EP, N., X, P., A, S., H, Y., and R, G.: The MERRA-2 Aerosol Assimilation, Technical Report Series on Global Modeling and Data Assimilation, 45, 2016.

Rogers, R., and Yau, M.: A short course of cloud physics. Pregamon, in, Oxford, 1989.

55   Schneider, T., Smith, K. L., O'Gorman, P. A., and Walker, C. C.: A Climatology of Tropospheric Zonal-Mean Water Vapor Fields and Fluxes in Isentropic Coordinates, Journal of Climate, 19, 5918-5933, 10.1175/jcli3931.1, 2006.

Sekiguchi, M., Nakajima, T., Suzuki, K., Kawamoto, K., Higurashi, A., Rosenfeld, D., Sano, I., and Mukai, S.: A study of the direct and indirect effects of aerosols using global satellite data sets of aerosol and cloud parameters, Journal of Geophysical Research: Atmospheres, 108, n/a-n/a, 10.1029/2002JD003359, 2003.

Shipway, B. J., and Hill, A. A.: Diagnosis of systematic differences between multiple parametrizations of warm rain microphysics using a kinematic framework, Quarterly Journal of the Royal Meteorological Society, 138, 2196-2211, 10.1002/qj.1913, 2012.

Sinclair, M. R.: An objective cyclone climatology for the Southern Hemisphere, Monthly Weather Review, 122, 2239-2256, 1994.

Sourdeval, O., Labonnote, L. C., Baran, A. J., Mülmenstädt, J., and Brogniez, G.: A Methodology for Simultaneous Retrieval of Ice and Liquid Water Cloud Properties. Part II: Near-global Retrievals and Evaluation against A-Train Products, Quarterly Journal of the Royal Meteorological Society, 2016.

Stevens, B., and Feingold, G.: Untangling aerosol effects on clouds and precipitation in a buffered system, Nature, 461, 607-613, 2009.

Stevens, B.: Rethinking the Lower Bound on Aerosol Radiative Forcing, Journal of Climate, 28, 4794-4819, doi:10.1175/JCLI-D-14-00656.1, 2015.

Thompson, G., and Eidhammer, T.: A Study of Aerosol Impacts on Clouds and Precipitation Development in a Large Winter Cyclone, Journal of the Atmospheric Sciences, 71, 3636-3658, 10.1175/JAS-D-13-0305.1, 2014.

Trenberth, K. E., and Stepaniak, D. P.: Covariability of Components of Poleward Atmospheric Energy Transports on Seasonal and Interannual Timescales, Journal of Climate, 16, 3691-3705, 10.1175/1520-0442(2003)016<3691:cocopa>2.0.co;2, 2003.

Trenberth, K. E., Fasullo, J., and Smith, L.: Trends and variability in column-integrated atmospheric water vapor, Climate dynamics, 24, 741-758, 2005.

Twomey, S.: INFLUENCE OF POLLUTION ON SHORTWAVE ALBEDO OF CLOUDS, Journal of the Atmospheric Sciences, 34, 1149-1152, 10.1175/1520-0469(1977)034<1149:tiopot>2.0.co;2, 1977.

Walters, D., Boutle, I., Brooks, M., Melvin, T., Stratton, R., Vosper, S., Wells, H., Williams, K., Wood, N., Allen, T., Bushell, A., Copsey, D., Earnshaw, P., Edwards, J., Gross, M., Hardiman, S., Harris, C., Heming, J., Klingaman, N., Levine, R., Manners, J., Martin, G., Milton, S., Mittermaier, M., Morcrette, C., Riddick, T., Roberts, M., Sanchez, C., Selwood, P., Stirling, A., Smith, C., Suri, D., Tennant, W., Vidale, P. L., Wilkinson, J., Willett, M., Woolnough, S., and Xavier, P.: The Met Office Unified Model Global Atmosphere 6.0/6.1 and JULES Global Land 6.0/6.1 configurations, Geosci. Model Dev., 10, 1487-1520, 10.5194/gmd-10-1487-2017, 2017.

Wang, Y., Wang, M., Zhang, R., Ghan, S. J., Lin, Y., Hu, J., Pan, B., Levy, M., Jiang, J. H., and Molina, M. J.: Assessing the effects of anthropogenic aerosols on Pacific storm track using a multiscale global climate model, Proceedings of the National Academy of Sciences, 111, 6894-6899, 10.1073/pnas.1403364111, 2014.

Wentz, F. J.: A 17-yr climate record of environmental parameters derived from the Tropical Rainfall Measuring Mission (TRMM) Microwave Imager, Journal of Climate, 28, 6882-6902, 2015.

Wielicki, B. A., Barkstrom, B. R., Harrison, E. F., III, R. B. L., Smith, G. L., and Cooper, J. E.: Clouds and the Earth's Radiant Energy System (CERES): An Earth Observing System Experiment, Bulletin of the American Meteorological Society, 77, 853-868, 10.1175/1520-0477(1996)077<0853:catere>2.0.co;2, 1996.

Wood, R.: Stratocumulus Clouds, Monthly Weather Review, 140, 2373-2423, 10.1175/MWR-D-11-00121.1, 2012.

Zhang, R., Li, G., Fan, J., Wu, D. L., and Molina, M. J.: Intensification of Pacific Storm Track Linked to Asian Pollution, Proceedings of the National Academy of Sciences of the United States of America, 104, 5295-5299, 2007.

Table 1 The coefficients for equation 1 based on using CDNC$_{SW}$ observed by MODIS and inferred from MERRA2 sulfate. Coefficients (a-d) are listed for each. The number of observations used to train the model is listed as n. The correlation coefficient, r, between predicted and observed CLWP is also listed for each model.

	a	b	c	d	n	r
MODIS	21.79	0.95	0.11	18.52	37837	0.79
MERRA2	19.23	0.86	0.19	4.53	49361	0.82

22

**CERES 3-hour Albedo Over Oceans Jan 2005**
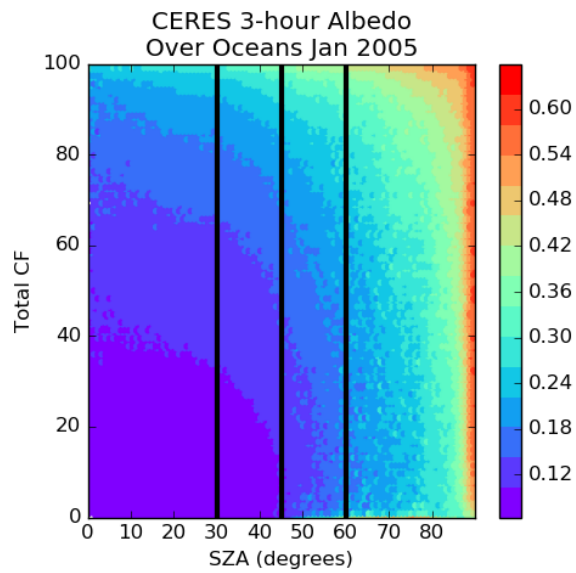
Fig. 1 CERES albedo over oceans binned as a function of cloud fraction and solar zenith angle (SZA) during January 2005. Above a SZA of 45° a strong dependence of albedo on SZA is seen. The SZA cut offs used in this study of 30°, 45° and 60° are shown with vertical black lines. Example CERES albedo is shown in Fig. S1.

5

23

(a) CLWP MAC-LWP

(b) CLWP HR (100 cm-3)

(c) CLWP HR (NH2000 cm-3)

(d) CLWP LR (100 cm-3)

24
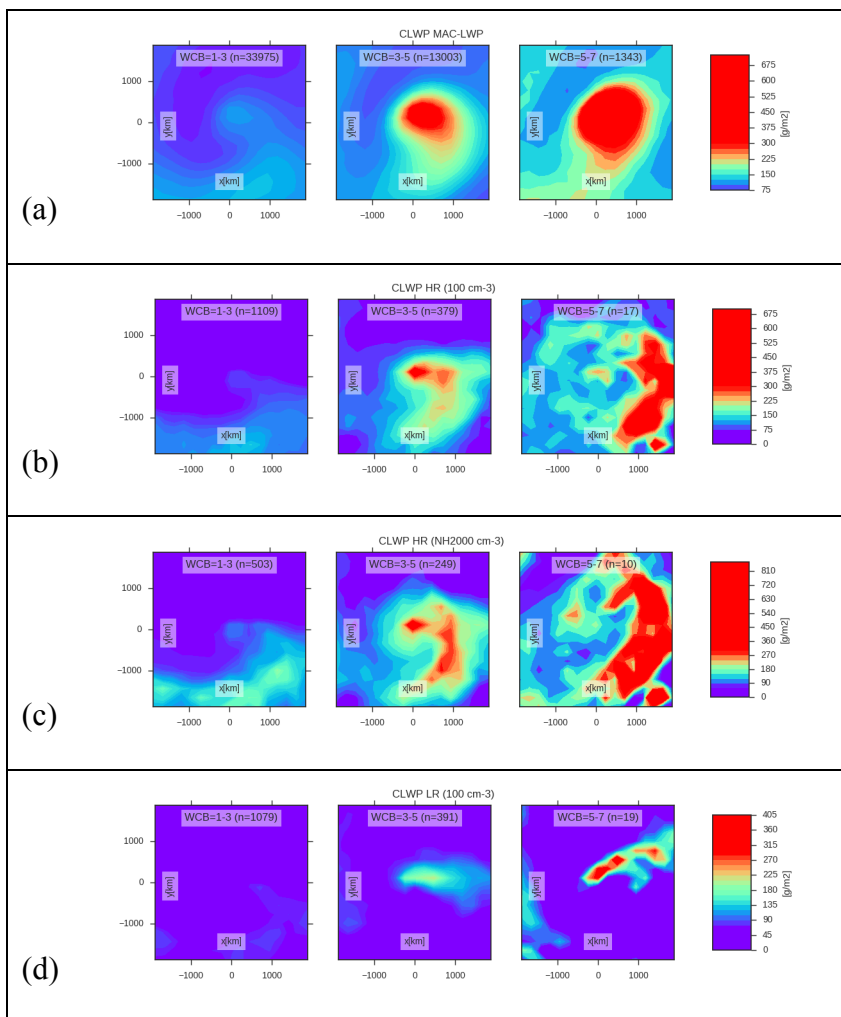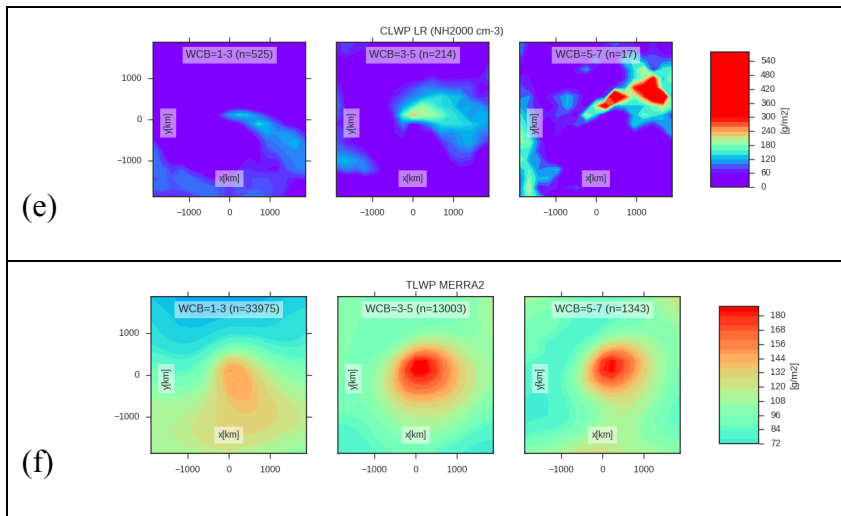
Fig. 2 Cyclone composites showing CLWP from (a) MAC-LWP, (b-c) the convection-permitting simulation in the control and enhanced CCN experiments, (d-e) the GCM-surrogate simulation in the control and enhanced aerosol experiments, and (f) MERRA2. All composites are shown in three bins of WCB moisture flux so that cyclones with similar meteorology can be compared. Note that plotted ranges differ between models and observations. The number of cyclones contributing to the mean composite are noted in each subplot.
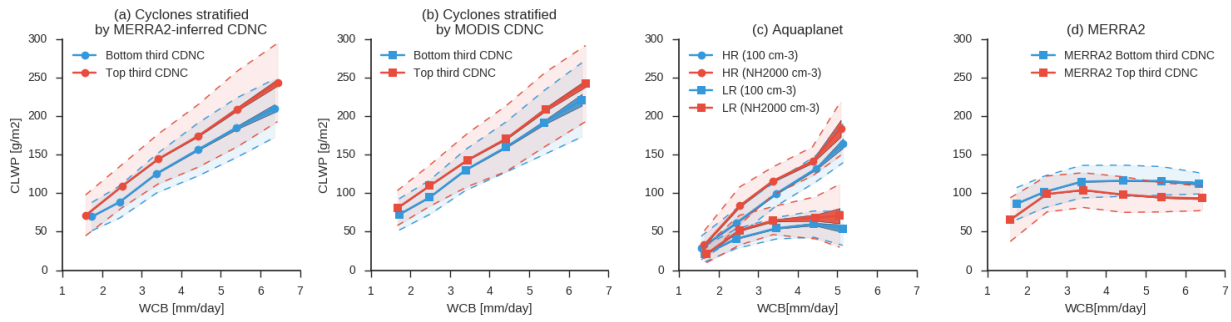
Fig. 3 Comparison between the dependence of cyclone mean liquid water path (CLWP) on warm conveyor belt (WCB) moisture flux as a function of increasing aerosol. The CLWP is binned by WCB moisture flux. The standard deviations in CLWP across bins are shown as shading. The standard error in the mean is shown thick solid lines. Figures (a) and (b) show MAC-LWP observations from 2003 to 2015 stratified by MERRA2-inferred $CDNC_{SW}$ and (b) stratified by observations of $CDNC_{SW}$ from MODIS. Panel (c) shows the simulated CLWP in a suite of global aquaplanet simulations split into low and high CCN simulations. In the aquaplanet simulations a high aerosol channel is added to the northern hemisphere to investigate the response of cyclone properties and surface accumulation mode aerosol concentrations are noted in the legend. Aquaplanet simulations are run at convection-permitting (HR) and GCM-surrogate resolution (LR). Panel (d) shows MERRA2 total precipitable liquid stratified by MERRA2-inferred $CDNC_{SW}$. In (a,b, and d) cyclones with $CDNC_{SW}$ in the top and bottom third of observed $CDNC_{SW}$ (see Fig. 4) are indicated by red and blue lines.
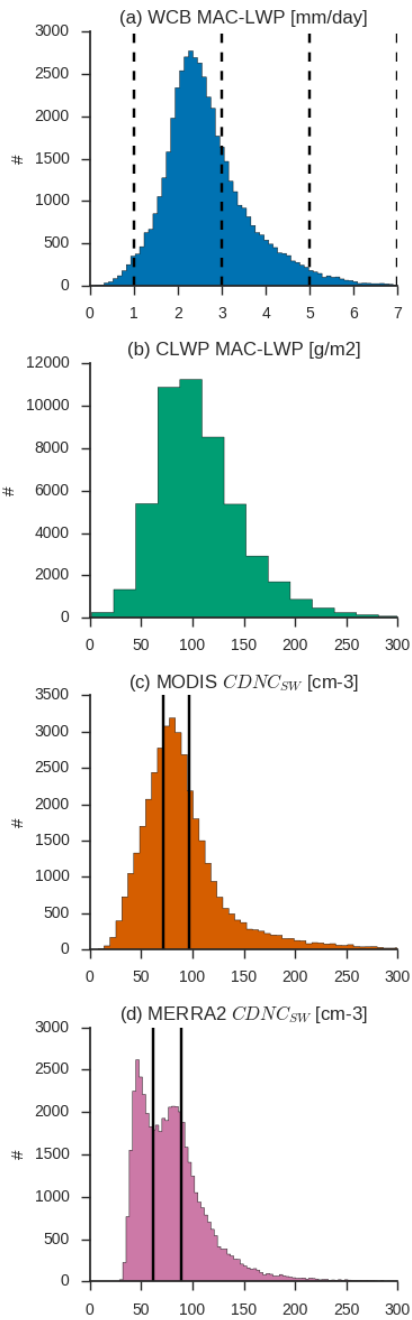
Fig. 4 Distributions of cyclone-mean properties within the 2003-2015 observational record. Units are noted for each variable. The number of composite cyclones with that value is indicated on the ordinate. Warm conveyor belt moisture flux is shown in (a). Cyclone LWP (precipitating and non-precipitating liquid) is shown in (b). Observations and MERRA2-inferred values of CDNC in the southwest quadrant of the cyclone (CDNC_SW) are shown in (c-d). In (c) and (d) the top and bottom third of distribution are indicated with dashed lines. In (a) WCB bins are shown with dashed lines.

27
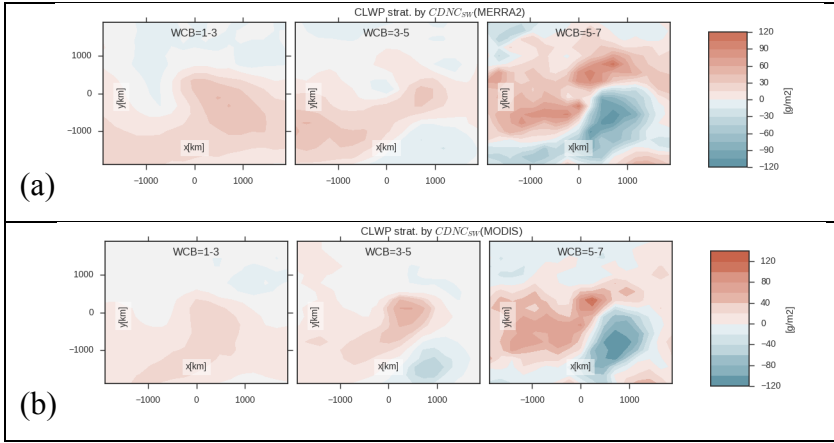
Fig. 5 The difference in cyclone composited MAC-LWP CLWP between the top and bottom third of CDNC$_{SW}$ inferred from MERRA2 (a) and observed by MODIS (b). Composites are shown split into WCB categories as in Fig. 2.
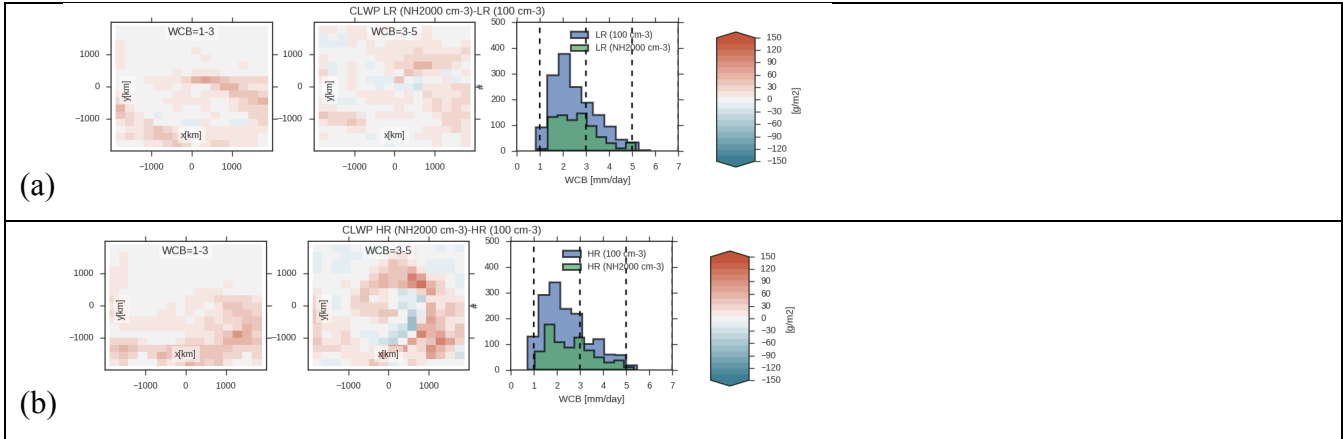
Fig. 6 The difference in mean cyclone composites between the high and low CCN simulations for (a) the GCM-surrogate low-resolution (LR) simulation and (b) the convection-permitting (HR) simulation. Differences in mean cyclone composites for different WCB regimes are shown. It should be noted that the relatively short integration time (relative to the observations) of the simulations did not yield a large number of cyclones with WCB>5 mm/day and only the first two WCB regimes are shown in contrast to Fig. 5. The distribution of cyclones by WCB in the simulations is shown on the rightmost plot.
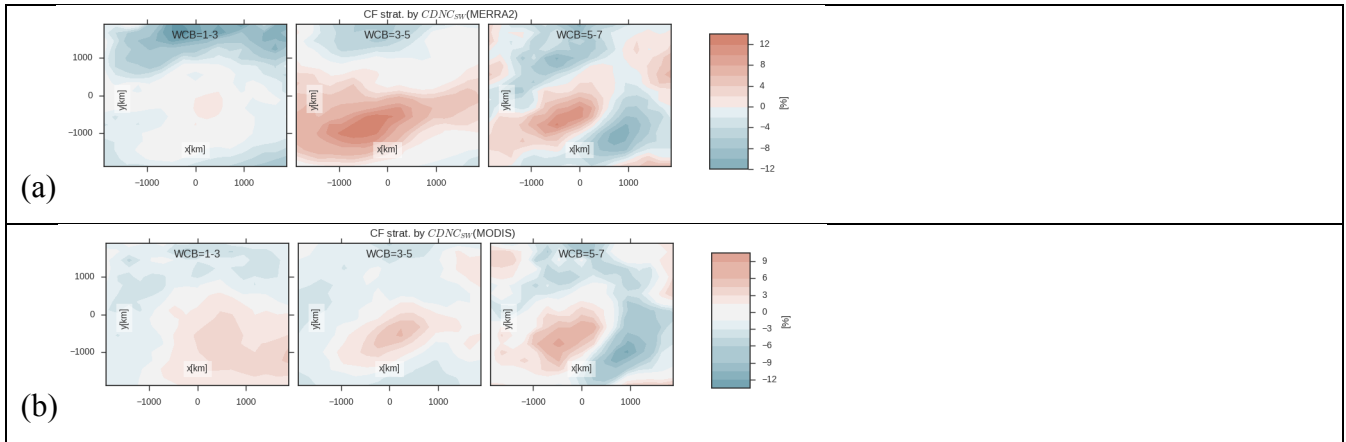
Fig. 7 As in Fig. 5, but showing differences in cloud fraction.
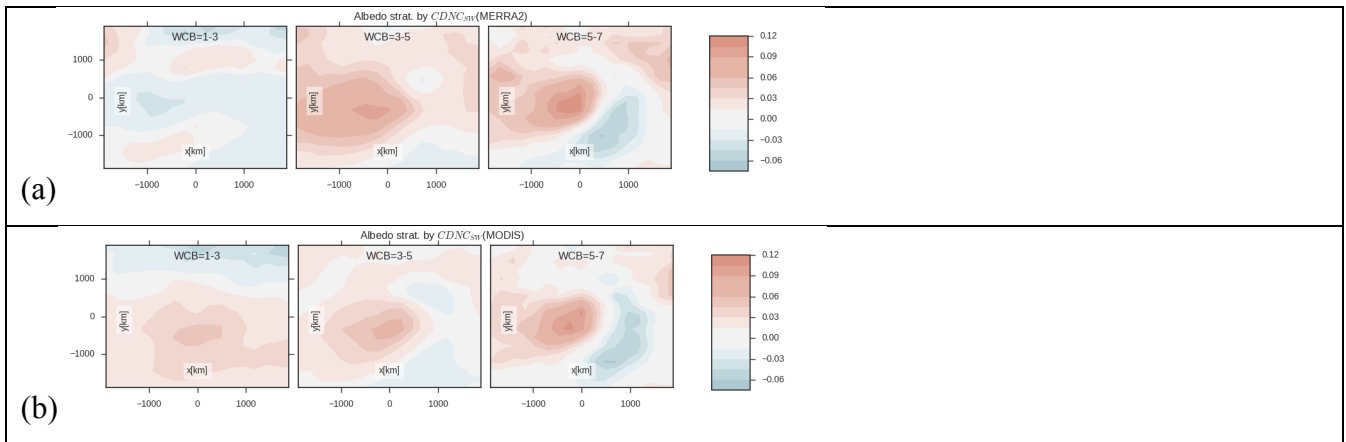
5   **Fig. 8 As in Fig. 5, but showing differences in albedo.**

29
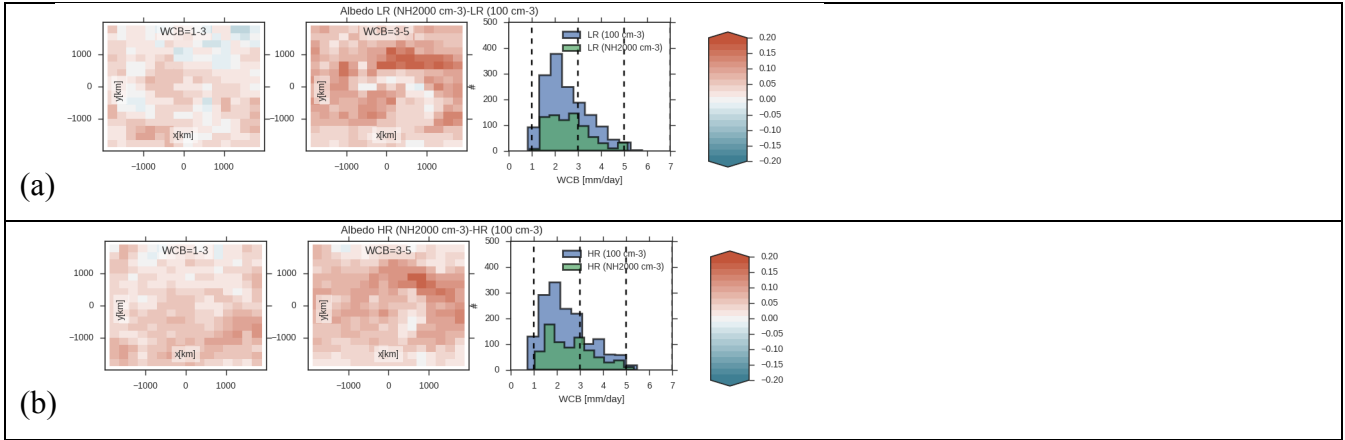
**Fig. 9** As in Fig. 6, but showing differences in albedo.
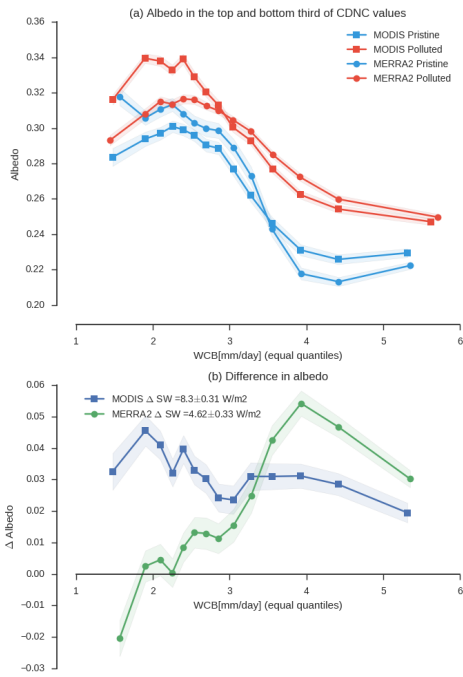
Fig. 10 (a) Cyclone-mean albedo from CERES as a function of WCB moisture flux. Data is shown binned into equal quantiles of WCB moisture flux and separated into the top and bottom third of observed $CDNC_{SW}$. Standard error in the mean is shown using shading. Both MERRA2 sulfate and MODIS-observed $CDNC_{SW}$ are used to partition the top and bottom third of $CDNC_{SW}$ and are noted in the legend. (b) shows the difference in albedo between the top and bottom third of observed $CDNC_{SW}$ as a function of WCB moisture flux. The mean difference in reflected SW based on this difference in albedo is noted in the legend. The albedo is scaled by the annual-mean climatological insolation between 30°-80° to calculate the reflected SW. Because albedo is a strong function of solar zenith angle (SZA) only 3-hourly measurements with SZA<45° are considered here (similar calculations using cut-offs of 30°, 60°, and 90° are shown in Fig. S10,11,12).
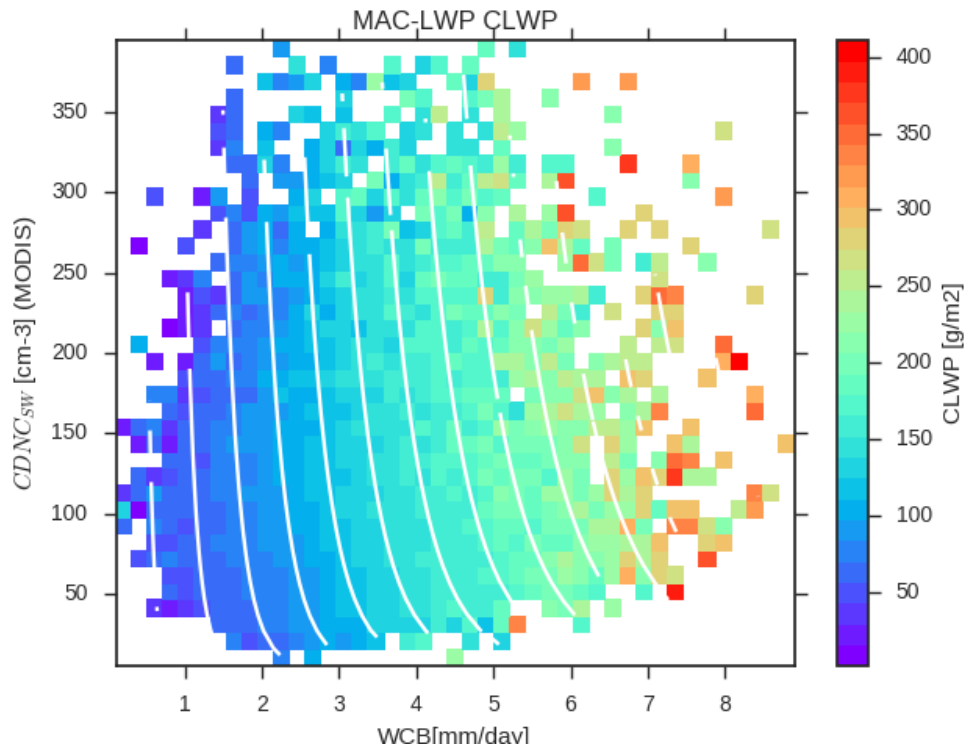
Fig. 11 The cyclone-mean CLWP in units of mm of liquid water observed by MAC-LWP binned as a function of WCB moisture flux and the CDNC$_{SW}$ observed by MODIS. Data is binned into equal size bins for the purpose of visualizing the data record. White lines show contours of constant CLWP as predicted by Eq. 1 and the coefficients listed in Table 1. The dependence of CLWP on CDNC$_{SW}$ inferred from MERRA2 is shown in Fig. S13.
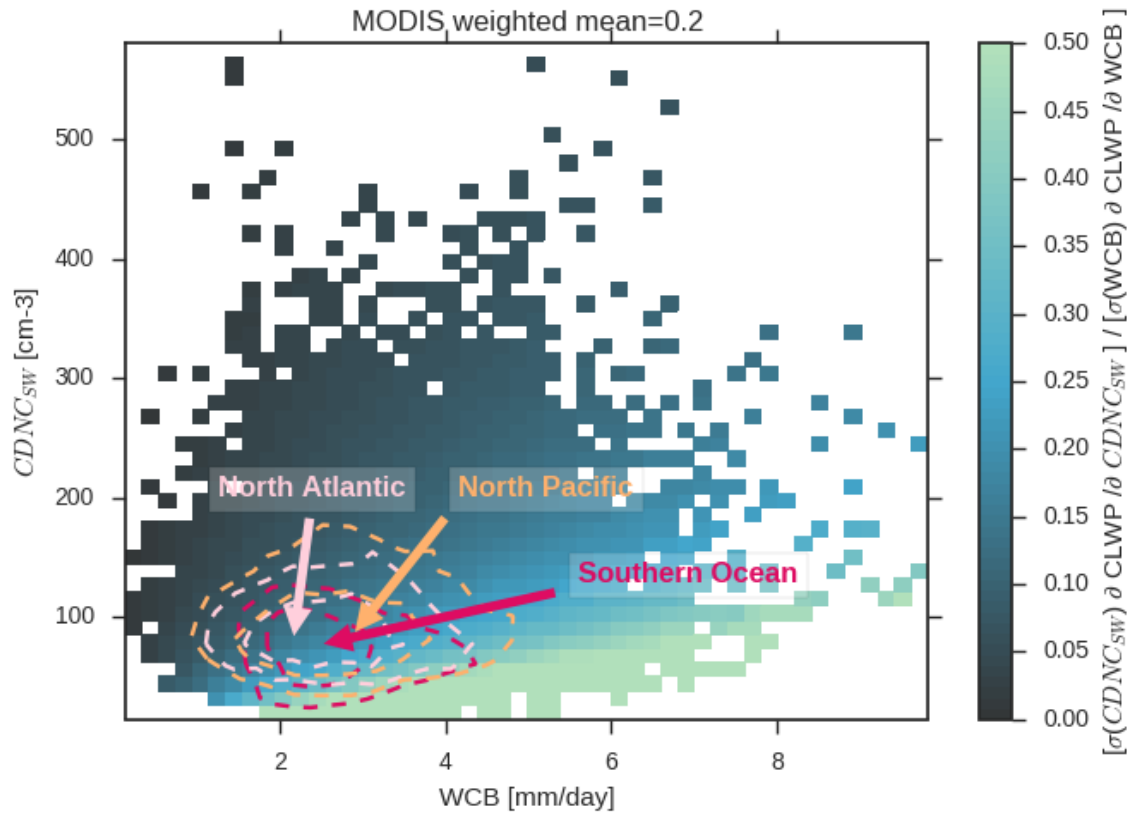
Fig. 12 The relative contribution to CLWP of perturbations in $CDNC_{SW}$ and perturbations in WCB as estimated using Eq. 1 and the standard deviation of each predictor over the historical record. The regression model was trained using MODIS-observed $CDNC_{SW}$ (the same plot is shown for MERRA2-inferred $CDNC_{SW}$ in Fig. S14). The partial derivative of Eq. 1 is taken with respect to each predictor and scaled by the standard deviation of that predictor. The ratio of the partial derivative scaled by standard deviations in each of the predictors is shown using colors. The joint probability distribution of cyclones during the observational record for different ocean regions are roughly indicated using dashed lines. The joint probability distribution of all observations is used to calculate the weighted mean of the fractional contribution of perturbations in $CDNC_{SW}$ and WCB over the range of WCB and $CDNC_{SW}$ in the observational record.